A Realistic Rotorcraft Noise Footprint Computation for Low-Noise Trajectory Optimization

Pierre Dieumegard, Frédéric Guntzer, Julien Caillet, Sonia Cafieri

A Realistic Rotorcraft Noise Footprint Computation for Low-Noise Trajectory Optimization

Pierre Dieumegard
PhD Candidate

Frédéric Guntzer
Acoustics Expert

Julien Caillet
Acoustics Expert

Airbus Helicopters
Marignane, France

Sonia Cafieri
Professor
ENAC, Université de Toulouse
Toulouse, France

ABSTRACT

This paper introduces recent developments in the computation of rotorcraft noise footprint, implemented in an Airbus Helicopters' internal software. The paper presents the main ingredients that have led to enhance the efficiency and accuracy of such noise footprint computation. This includes taking into account both the particularities of turns in noise emission and the influence of the wind on noise propagation. Furthermore, the software is able to assess a real traffic environmental impact, since computations are done within a realistic 3D simulation environment, taking into account both the curvature of the Earth and the topography of the ground. A variety of noise annoyance indicators can be computed thanks to the coupling with demographic and background noise data. Such realistic noise footprint computation is embedded in a tailored algorithmic scheme aiming at optimizing rotorcraft trajectories in such a way that their associated noise footprint is minimized. The proposed optimization approach has been tested on multiple real-world case studies, showing significant prospective noise reduction compared to reference trajectories.

INTRODUCTION

Rotorcraft are essential to conduct specific missions that other types of aircraft cannot perform, such as Emergency Medical Services (EMS), civil transportation to Oil and Gas (O&G) platforms, or surveillance missions. However, community acceptance of rotorcraft operations remains limited due to the resulting noise. In addition to existing helicopter traffic, an increase in rotorcraft operations above urban areas is foreseen, especially with the emergence of future Urban Air Mobility (UAM). As noise remains today one of the main issues to the development of such operations, reducing the noise impact of rotorcraft operations is urgently needed. Emitted noise can be reduced by modifying the design of rotorcraft (Refs. 1, 2), but this usually implies a long-time development process. As the emitted noise strongly depends on rotorcraft operating conditions, flying optimal low-noise trajectories can help improving community acceptance.

The design of low-noise rotorcraft operations relies on the evaluation of the noise footprint of rotorcraft trajectories. In this paper we present the recent improvements in the accuracy and efficiency of the noise footprint computation, that is performed through an Airbus Helicopters' software. This noise footprint computation is based on and extends the work presented in (Ref. 3), comprising the computation of the noise emission and of the noise propagation for a given rotorcraft.

In the literature, numerical simulations, aiming at estimating rotorcraft community noise impact, are based on more or less accurate physical modeling of rotorcraft noise emission and noise propagation to the ground. In many studies, such noise modeling is only accurate for steady flight conditions (Refs. 4, 5) and does not capture the impact of maneuvers on the radiated noise. Using such noise models to design optimal trajectories may lead to unintended low-noise trajectories with strong changes in flight conditions (Ref. 6), for which the noise impact is underestimated. On the other hand, very realistic noise models exist (Ref. 7) but often imply huge computational effort, that prevent them to be used within an optimization algorithm for the design of low-noise trajectories with a reasonable computational cost. In this paper, we present a performing noise emission and propagation computation, which features a good compromise between accuracy of the noise footprint and computational time.

The noise impact on population relying on this computation constitutes the optimization criterion in our design of optimal trajectories. As derivatives cannot be computed for such a criterion function, the problem is a so-called *black-box* optimization problem. To solve the optimal trajectory problem, population-based methods are typically used (Refs. 3, 4). However, in the framework of black-box

optimization, these methods remain computationally very expensive. Recent works resort to more efficient heuristic methods based on space discretization, such as A* (Refs. 5,8). However, such constructive algorithms assume that noise is factorable (Ref. 5), while it is not. In this paper, we address the problem of low-noise rotorcraft trajectory design using a performing optimization method for black-box optimization problems, providing a guarantee of local optimality.

Rotorcraft noise abatement procedures design has been widely studied in the literature (Refs. 3–5, 8, 9). Most of the works address the optimization of 2D approach profiles by focusing on avoiding Blade-Vortex Interaction (BVI) noise (Refs. 3, 4, 6, 9). In (Refs. 8, 10) and references herein, 3D trajectories are considered, but the study remains either limited to short single parts of the trajectory (e.g. level turn, straight approach) or defined in an unrealistic simulated environment. In this paper, we optimize both the rotorcraft lateral and longitudinal path along with its speed.

The paper is structured as follows. First, we introduce the recent developments and capabilities of the noise footprint computational chain so as to be able to perform realistic environmental impact assessment. Then, we present how we embed this computational chain in a dedicated algorithmic scheme to provide low-noise optimal trajectories. The final section presents and discusses numerical results obtained with the proposed approach on real-world instances.

AN ACCURATE AND EFFICIENT NOISE FOOTPRINT COMPUTATIONAL CHAIN

The noise footprint computational chain considered in this paper is named CAROT (Compute Acoustics of a Rotorcraft Over Terrain) and relies on the work presented in (Ref. 3). An aeroacoustic database has been built from dedicated flight tests measurements of rotorcraft noise in multiple steady-state flight conditions. The developed software is able to evaluate the noise footprint of a given rotorcraft trajectory defined in a local coordinate system. The trajectory is sampled in equally time-spaced emission instants. Every considered emission instant is linked to a steady-state flight condition. True Air Speed (TAS) v and aerodynamic slope γ are used as noise governing parameters to retrieve the emitted noise data from the aeroacoustic database. Additional effects of acceleration/deceleration as well as wind effect on noise emission are taken into account through a quasi-static approach as in (Ref. 6). The emitted noise data is then propagated to a set of user-fixed positions on the ground. A typical value for trajectory sampling that is used for rotorcraft noise certification is 0.5s. The lower the time step, the more accurate the computation, but the higher the computing time. Recent developments aiming at improving the computational efficiency are presented at the end of the section. First, we detail the recent software upgrades including the effect of wind on noise propagation and the particularities of turning flight.

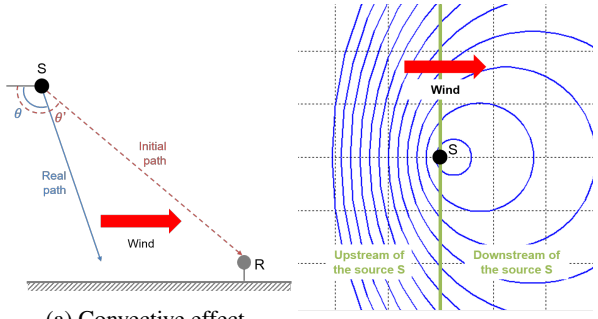

(a) Convective effect

(b) Convective amplification for a wind speed of M=0.5

Figure 1. Representation of the convection effect on noise propagation.

Wind influence

The effect of wind on the noise footprint associated to a rotorcraft trajectory is twofold as detailed in (Ref. 11). First, wind has an influence on the flight mechanics of rotorcraft: it modifies rotorcraft's True Air Speed, advance ratio, main rotor tip-path-plane angle of attack, etc. and therefore the rotorcraft acoustic source. This effect on noise emission is already handled in the computational chain. More details are given in (Ref. 3). Furthermore, wind has also a non-negligible effect on noise propagation. Specifically, there are three different effects:

- *Convective effect.* The acoustic wave fronts are convected with the wind. For an acoustic wave propagating in the direction of the flow (i.e. downstream of the source), the wave is *carried* by the flow, hence travelling a shorter distance in the air (blue path) to reach the receiver, as illustrated in Figure 1a. Such a decrease in the propagation distance lead to a decrease in the noise attenuation, thus an increase in the noise amplitude on the ground. On the contrary, for an acoustic wave propagating in the opposite direction of the flow (i.e. upstream of the source), the propagating distance in the air is longer. This leads to an increase of the noise attenuation, thus a decrease in the noise amplitude on the ground.
  Figure 1a also shows that there is a change in the directivity of the source considered for propagation. The observation angle θ should be considered instead of θ'.

- *Convective amplification.* The wind affects also sound celerity with respect to ground. Compared to a situation with no wind, the sound celerity with respect to ground is lower (respectively higher) upstream (resp. downstream) of the source. This leads to an asymmetrical propagation: wave fronts are closer (resp. further) to each other upstream (resp. downstream) of the source, as illustrated in Figure 1b. Therefore, the noise amplitude perceived upstream (resp. downstream) of the source is higher (resp. lower) than without wind.

We observed that these two phenomena, shown in Figure 1, have a significant effect on noise amplitude at the receiver for

very high unrealistic wind velocities (Mach ≥ 0.5). For usual wind conditions, the convective effect and the convective amplification remain slight and tend to balance out. They will indeed be neglected in the following. However, the change in the directivity of the source is computed and taken into account since it can reach up to 5°.

- *Refraction.* According to the International Standard Atmosphere (ISA), the temperature varies with altitude following a given temperature gradient that thus creates a sound celerity gradient with altitude. The latter is additionally affected by the presence of a wind gradient and has a strong impact on noise propagation. In particular, it can cause the bending of the acoustic rays as illustrated in Figure 2a. According to Snell-Descartes law, the acoustic rays are deflected to areas where the sound celerity is lower. In the presence of wind and assuming that wind gradient with height is positive, the sound celerity decreases with altitude (see the violet curve in Figure 2a) for acoustic waves propagating upstream of the source. Under these specific conditions, such acoustic rays are refracted upward, leading to the appearance of shadow zones (i.e. silent zones), as represented in Figure 2b. The presence of a shadow zone turns out to be of great interest when addressing operational noise reduction on the ground.

The different effects of the wind on noise propagation have been integrated to the computational chain CAROT. As detailed above, it was considered that the convective effect and convective amplification offset each other for usual wind conditions. CAROT thus implements a refraction model based on Nord2000 standard that indicates the presence or not of a shadow zone. This simplified model considers a linear sound celerity profile interpolated from the real one and assumes that the acoustic rays are circular. The model remains fairly limited compared to more complex ray tracing algorithms but it reveals to be efficient to compute the shadow zone. It will be further used in the scope of rotorcraft trajectories optimization, where the shadow zone might play a significant role to reduce noise exposure.

Figure 3 shows the CAROT-computed SEL noise footprint (5dB(A) contours) associated to a rotorcraft straight approach flight in several wind conditions. We observe that the presence and the size of the shadow zone (white areas) is highly dependent on the wind. In particular, Figures 3a, 3b and 3c show the influence of the wind speed on the size of the shadow zone: the higher the wind speed, the larger the shadow zone. The shadow zone is also highly dependent on the height of the rotorcraft due to the bending of the acoustic rays: the lower the rotorcraft, the closer the shadow zone. In addition, Figures 3c and 3d show the influence of the wind direction on the geometry of the shadow zone. In the scope of low-noise trajectory design, in windy conditions, such shadow zones could be used to further reduce the noise impact on sensitive areas.

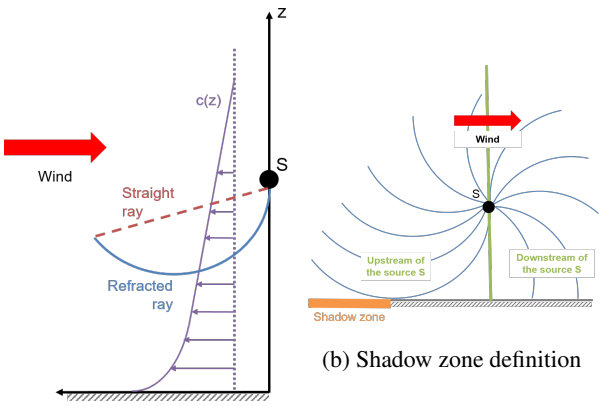

(a) Refraction effect

(b) Shadow zone definition

Figure 2. Representation of the bending of the acoustic rays in windy conditions.

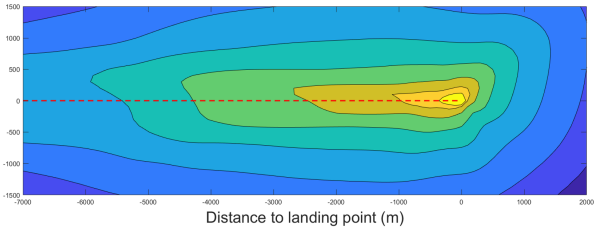

(a) No Wind

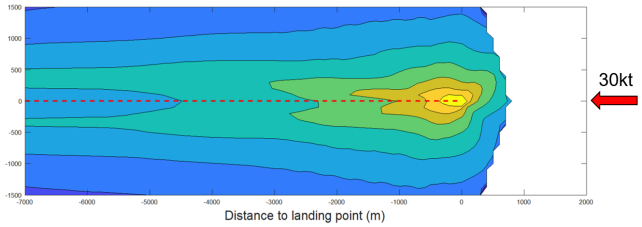

(b) Head wind (90°), 30kt

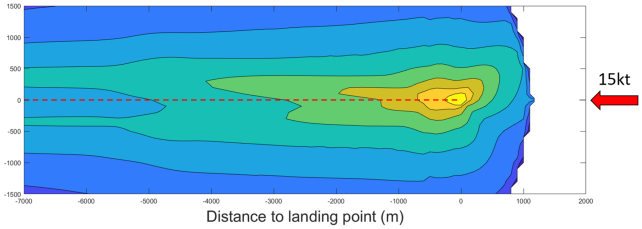

(c) Head wind (90°), 15kt

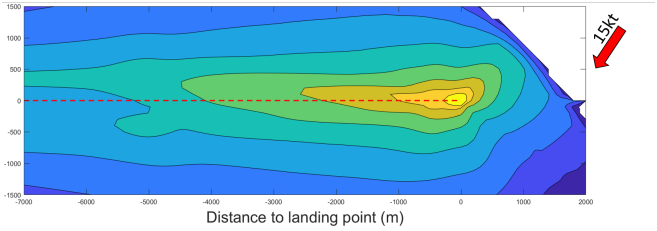

(d) Side wind (30°), 15kt

Figure 3. SEL noise footprint (5dB(A) contours) of a rotorcraft straight approach in various wind conditions.

Turning flight

In addition to the inclusion of the wind effect on noise propagation, a study of the noise emission during turning flight has

been performed. According to literature, the noise emitted during turns presents special features (Refs. 12, 13) compared to straight flight. In particular, the radiated noise might reach very high levels (Ref. 14), especially during transient maneuvers (e.g. roll-in). In this paper, we do not take into account the effect of transient maneuvers, as it is assumed that they remain negligible compared to the whole duration of the flights that we seek to optimize.

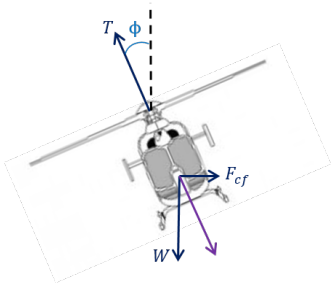

Figure 4. Lateral force balance for turning flight.

During a turn, the lateral force balance of the rotorcraft is modified (see Figure 4) as a new contribution occurs: the centrifugal force, denoted F_{cf}. In order to balance the combined contribution of the rotorcraft weight W and such outward centrifugal force, the thrust T must be increased with respect to straight level flight. Therefore, the noise governing parameters (v, γ) that were used in (Ref. 3) might not be sufficient to model the noise radiated during turning flight. Most of the papers in the literature (Refs. 12–14) propose to consider the thrust coefficient C_T, in addition to the true air speed v and the aerodynamic slope γ, as another noise governing parameter.

Several numerical simulations through a comprehensive tool chain (HMMAP) have been performed in order to see the influence of the thrust coefficient on the noise emitted by the main rotor. The tool chain is first composed of Airbus Helicopters' flight mechanics tool HOST (Ref. 15) and ONERA's free wake model MESIR. The rotorcraft trim computation performed through HOST is strongly coupled with the balance of the main rotor wake computed through MESIR. Then, the wake roll-up is computed through MENTHE and the Blade-Vortex interactions are estimated through ARHIS. Finally, the blade pressures and resulting acoustics are estimated according to Ffowcs Williams-Hawkings (FWH) model through PARIS. Further details about the whole HMMAP tool chain can be found in (Ref. 16). All the simulations have been performed with a H130 main rotor model.
General trends, that have been drawn out from these simulations, are consistent with literature (Refs. 12–14):

- The noise levels on the advancing blade side are higher than the noise levels on the retreating blade side.
- The turns towards the advancing blade side are noisier than the turns towards the retreating blade side.
- The higher the rate of turn, the higher the radiated noise.

Figures 5, 6 and 7 illustrate the HMMAP-calculated noise footprints of the H130 isolated main rotor trimmed in a 100kt turn, for different rates of turn (from 3°.s^{-1} to 9°.s^{-1}). For each figure, the top left (respectively top right) noise footprint shows the radiated noise for a turn towards the advancing (resp. retreating) blade side, whereas the bottom figure shows the noise footprint associated to the straight level flight. The rotorcraft is located at (X,Y)=(0;0) point, 150m above ground. The same color scale is used for all the noise footprints, with 1dB(A) per contour lines.

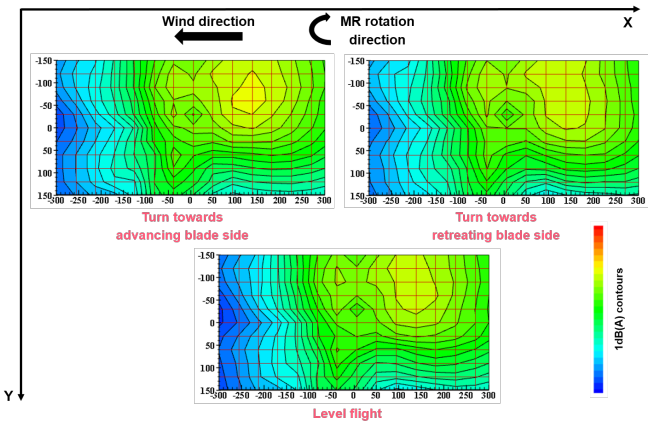

Figure 5. HMMAP-simulated noise footprint of isolated H130 main rotor (100kt - Rate-one turn 3°.s^{-1}), 1dB(A) per contour line.

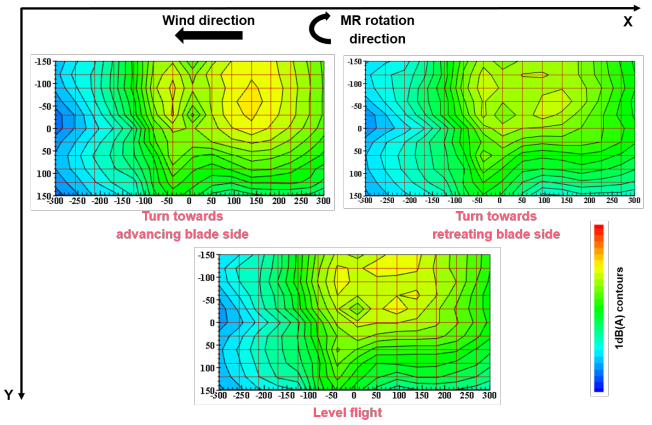

Figure 6. HMMAP-simulated noise footprint of isolated H130 main rotor (100kt - Rate-one turn 6°.s^{-1}), 1dB(A) per contour line.

Regarding the inclusion of the thrust coefficient as a noise governing parameter, different conclusions might be drawn depending on the rate of the turn considered. Figure 5 shows the simulation of the noise emitted by the main rotor of a H130 rotorcraft performing a 100kt turn with a 3°.s^{-1} rate of turn. We observe that, for such moderate rate of turn, the noise radiated during straight and turning flight present the same directivity patterns with comparable noise levels (lower than 1dB). In addition, we see that there is limited influence of the

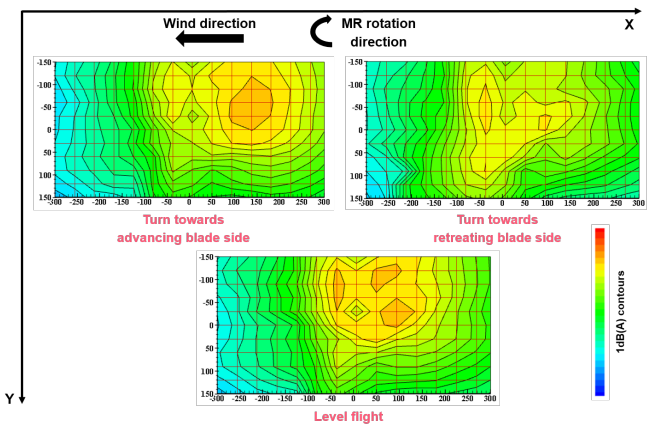

Figure 7. HMMAP-simulated noise footprint of isolated H130 main rotor (100kt - Rate-one turn 9°.s^{-1}), 1dB(A) per contour line.

side of the turn.

Figure 6 illustrates the simulation results for a 100kt rate-two turn (6°.s^{-1}). In that case, the bottom figure shows the noise footprint of the main rotor loaded with the same thrust coefficient than in turning flight. This is equivalent to considering a straight flight with a heavier rotorcraft. Figure 6 shows that an acoustic mapping with equivalent-C_T straight flight seems to be acceptable for moderate rate of turns. Such mapping consists in modeling the noise emitted by a rotorcraft in turning flight by the noise emitted by an heavier rotorcraft (i.e. having the same thrust coefficient C_T) in straight flight.

For turns with higher rate of turns (e.g. 9°.s^{-1}), this mapping is not valid anymore due to the dependency of the noise directivity to the side of the turn, as shown in Figure 7.

According to rotorcraft traffic analysis of turning flight performed on real flight data, the rate of turn remains below rate-one turn (i.e. 3°.s^{-1}) for more than 90% of the time. Therefore, in this paper, it is assumed that for the considered rotorcraft (H130) and conventional airspeed, TAS and the aerodynamic slope (v, γ) remain sufficient noise governing parameters even for turning flight.

Yet, the attitude of the rotorcraft is taken into account as it has a strong influence (especially for the bank angle) on noise levels on the ground. The noise footprint associated to a 100kt turn towards the advancing blade side, with a bank angle of 15° has been computed. The first computation considers that the rotorcraft remains horizontal during the turn (no attitude considered), while the second computation takes into account the roll of the rotorcraft. Figure 8 illustrates the significant differences (up to 4dB) in $L_{A,max}$ between both noise footprints. Such difference confirms that the attitude of the rotorcraft plays a significant role in the directivity of the emitted noise, hence on the noise footprint.

Finally, in the scope of this paper, the noise model remain governed by two flight parameters only (v, γ) but includes the attitude of the rotorcraft, which has a significant effect, especially during turning flight. This choice has been validated through flight test comparison. Several flight tests have been performed by a H130 helicopter turning left (i.e. towards the

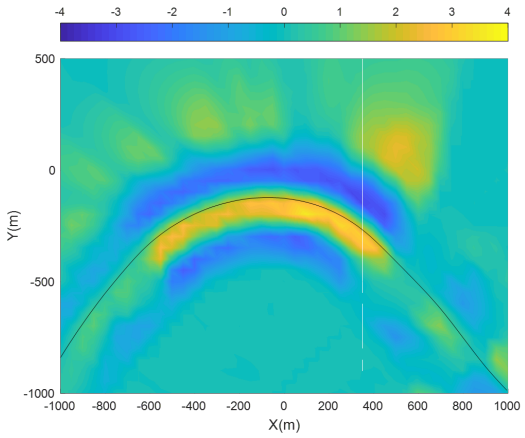

Figure 8. $\Delta L_{A,max}$(Banked Turn) - $L_{A,max}$(Horizontal Turn)

advancing blade side) over a regular array of microphones as part of the Friendcopter flight test campaign (Ref. 17). The different flight conditions of the stabilized turns are detailed in Table 1 and the associated flight tracks are plotted in Figure 9 over the microphone array.

Symbol key (Fig. 9)	True Air Speed (kt)	Bank angle (°)
···	70	15
—·	70	25
—	100	15
— —	100	25

Table 1. Turning flight tests description

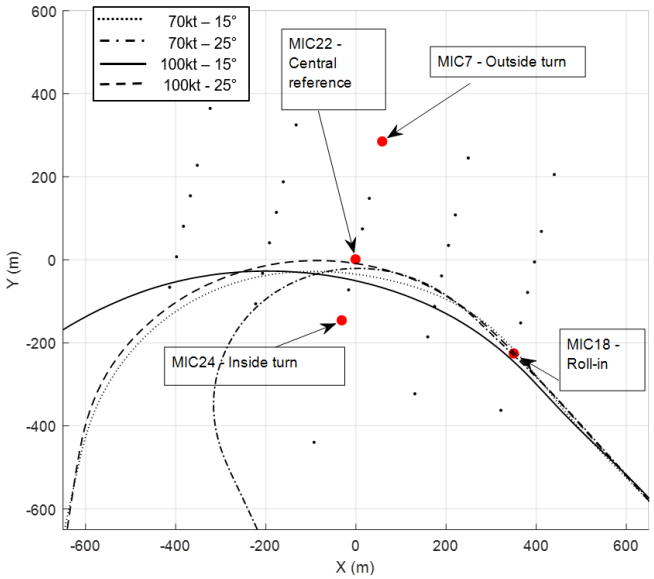

Figure 9. Illustration of the flight tracks and the microphone array.

Figure 10 presents the noise footprints ($L_{A,max}$) associated to both the noise levels measured through flight tests and simulated through the computational chain, which implements the modeling presented above. Figures 11 and 12 presents the

temporal evolution of the noise at four specific microphone locations, that are detailed in Figure 9. The three curves corresponds to the CAROT-simulated noise with roll correction (blue line), the CAROT-simulated noise without roll correction (red line) and the measured noise (yellow line). The figures shows that the simulation accounting for the attitude of the rotorcraft attitude is closer to the measure. In addition, Figure 11 confirms that the current modeling for the H130 is accurate enough for moderate turns (15°, $\sim 3°.s^{-1}$) and conventional airspeed. We observe that noise simulated through the software is very similar to the noise measured during the flight test (+/-2dB), validating our approach. For higher rate of turns, we see a tendency to overestimate the noise levels (see Figure 10b).

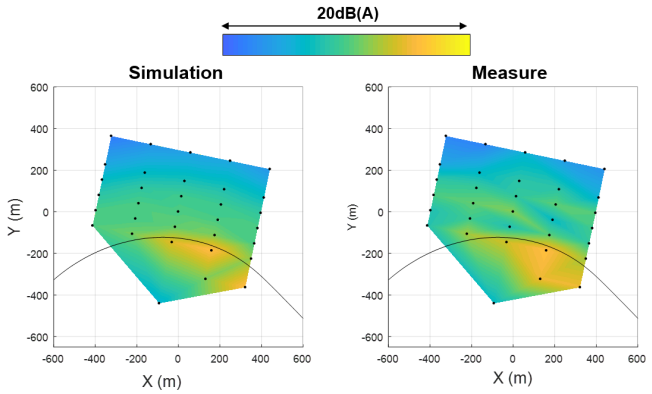

(a) 100kt - 15° Turn ($\approx 3°.s^{-1}$)

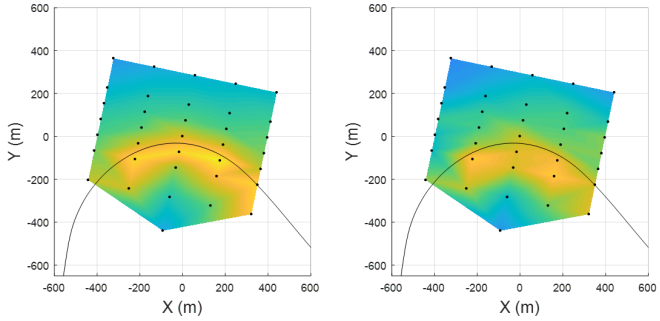

(b) 100kt - 25° Turn ($\approx 6°.s^{-1}$)

Figure 10. Noise footprint ($L_{A,max}$) of a rotorcraft turn at 100kt for different bank angles. Comparison between flight tests measurements and simulations.

We showed that for an H130 helicopter and conventional airspeed, the noise radiated during moderate turns ($\sim 3°.s^{-1}$) can be modeled by considering the banking of the rotorcraft only. This simplified model based on main rotor HMMAP-simulations have been validated through flight tests. In order to draw more general trends, some further studies should look on more conservative cases (higher airspeed), other types of rotorcraft and consider other noise sources (e.g. tail rotor, engines) than the main rotor only.

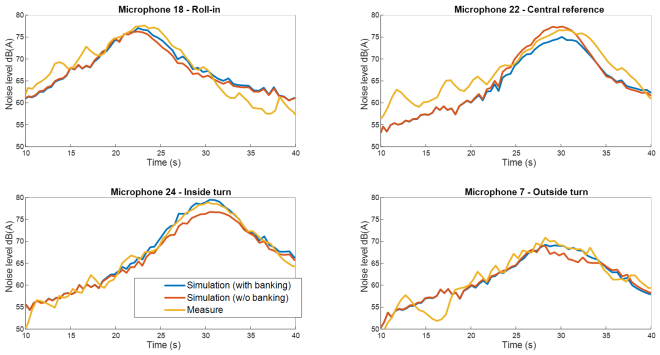

Figure 11. Temporal evolution of noise at four specific microphones (Turn towards the advancing blade side, 100kt, 15°).

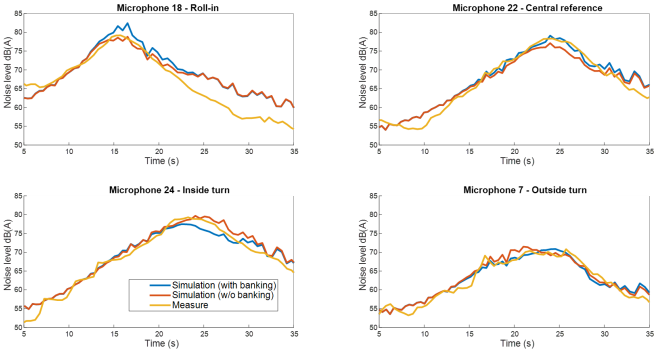

Figure 12. Temporal evolution of noise at four specific microphones (Turn towards the advancing blade side, 100kt, 25°).

Computational efficiency

The noise footprint of a rotorcraft trajectory is usually computed on a regular grid of ground positions. An illustration of such grid, with a typical sampling step of 100m, is given in Figure 13a. We recall that during the computation, the rotorcraft trajectory is sampled in a succession of equally time-spaced emission instants (typically every one second). For every emission instant, the computed emitted noise data is propagated to every ground position of the pre-defined regular grid. The computational complexity thus relies on the number of pairs (emission instant, ground position) for which noise emission and propagation are computed. The computational cost depends thus on two main factors: the sampling step of the trajectory and the sampling step of the regular grid. In order to keep a noise footprint computation with an acceptable precision, the increase in the sampling step, hence the reduction of the computational cost, remains limited. For local short trajectories, the computational cost is reasonable as the number of pairs to be computed remains small.
However, when assessing real traffic noise impact, the areas considered are significantly wider and the associated computational cost could dramatically increase. Yet, for such large scale studies, it is not required to compute noise emission and propagation for every pair (emission instant, ground position). Indeed, the computational chain has been updated to filter out only relevant pairs to be computed by setting a maximal

source-receiver distance. The value of this maximum propagation distance has been set to 3000m, which corresponds to a 43dB(A) noise level on ground, for the noisiest H130 flight condition. Such level is deemed to be negligible compared to the ambient noise in an outdoor environment. Figure 13 gives a 2D representation of a really flown trajectory (in red) over the set of ground positions (black dots) where the noise has been computed. Figure 13a shows the initial full grid of ground positions, while Figure 13b illustrates the relevant-only grid positions after filtering. We observe that there is a huge reduction in the amount of computed ground positions paving the way to computational cost reduction.

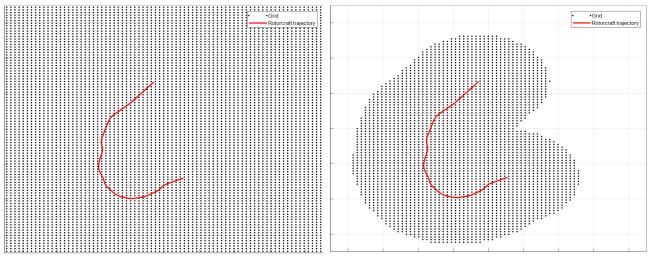

(a) Non-filtered computational grid (E/R max. distance = ∞)

(b) Filtered computational grid (E/R max. distance = 3000m)

Figure 13. Representation of the grid of ground positions where noise level is computed.

Furthermore, the emission/propagation loop has been translated into a compiled language (Fortran code) known to be more computationally efficient than an interpreted language such as Matlab. The additional reduction of the computing time is given in Table 2.

Table 2. Computational time savings.

Trajectory Number	Code version	Nb of computed E/R pairs	CPU time (s)
1	Original (full Matlab)	589589 (100%)	6.0
	Updated (full Matlab)	318260 (54.0%)	3.3
	Updated (with Fortran)		1.1
2	Original (full Matlab)	7062552 (100%)	141.5
	Updated (full Matlab)	683262 (9.7%)	13.9
	Updated (with Fortran)		9.4

Table 2 confirms the observation made in Figure 13 by giving the computational complexity of the noise footprint computation for two different trajectories. The first trajectory is a simple straight final approach flight over a flat ground, as considered previously when assessing the influence of noise on propagation, see Figure 3a. The second trajectory considers a large scale real approach flight to a given heliport, which will be considered for optimization in the following. Its 2D flight path is represented (in red) in Figure 13. Table 2 compares both trajectories in terms of the number of computed emission/reception (E/R) pairs and of computational time for the different versions of CAROT computational chain. The *original* version is the one introduced in (Ref. 3), while the *updated* version is based on the original one including the recent development presented in this paper. A distinction is made between the updated version keeping the original propagation loop based on the Matlab code and the updated version including the Fortran code.

All the tests have been performed on a Linux platform with 48 CPUs (3.00 GHz) and 130 GB RAM. We remark that the computational time remains small for local trajectories (e.g. Trajectory 1) even with the original version of the computational chain. However, Table 2 shows that for large scale studies, it is essential to filter out the relevant emission/reception pairs to be computed in order to keep a acceptable computational time. As an example, for the trajectory drawn in Figure 13, only very few original pairs (6.9%) are relevant for noise footprint computation. This more efficient computational chain allows us to perform larger scale noise impact assessment while keeping a reasonable computing time. Moreover, such reduction in the computational time is also beneficial in the scope of trajectory optimization for the evaluation of each candidate trajectory.

ENVIRONMENTAL IMPACT ASSESSMENT

The previous section presented the recent upgrades of the noise footprint computational chain, that improve both its accuracy and efficiency. To perform more realistic environmental impact assessment, the computational chain needs to be able to handle real traffic data and its simulation in a realistic environment. In addition, the tool has to be coupled with demographic data to get an evaluation of the noise impact on population. These further improvements with respect to the original version are presented in the next section with an example of traffic analysis in France.

3D realistic simulation environment

In the previous version of the computational chain (Ref. 3), only straight approaches over flat terrains were considered. In order to compute the noise footprint of 3D really-flown trajectories, a realistic simulation environment taking into account the curvature of the Earth is needed. Indeed, when assessing missions over wide areas, the assumption of a local flat Earth does not hold. Such a realistic simulation environment is defined according to the International Civil Aviation Organization (ICAO) standard World Geodetic System 1984 (WGS84), that comes with a widely used coordinate system. WGS84 also provides a reference geoid that defines the mean sea level: Earth Gravity Model 1996 (EGM96). Rotorcraft positioning is ensured by Global Navigation Satellite System (GNSS), which provides trajectory data in WGS84 coordinate system, i.e. latitude, longitude and height above WGS84 ellipsoid. The trajectories considered will thus be defined in this

format.

For the noise assessment of real trajectories, it is also necessary to consider real terrain elevation data rather than flat ground since it might significantly affect the sound propagation distance, which has a double contribution in noise attenuation. The digital elevation model considered is the Digital Terrain Elevation Data (DTED). Terrain elevation is described as the height above EGM96 geoid with a post spacing of approximately 90m (DTED level 1). Combining DTED and WGS84 information, the initial grid of ground positions is also defined in the WGS84 coordinate system, so as to be consistent with the trajectory definition.

More detailed topographic data, such as buildings geometry, is not handled by the presented computational chain. For more specific studies, such as the impact of future Unmanned Aerial Vehicles (UAVs) operations above cities, it is necessary to account for potential masking, reflection and diffraction effects caused by the presence of buildings. In that case, the computational chain has been coupled to a dedicated open-source tool: NoiseModelling (Ref. 18). This software produces environmental noise maps over large urban areas, accounting for such building effects. In this paper, we focus on designing low-noise trajectories for a specific type of rotorcraft: helicopters. Since helicopters fly at relatively high altitudes (at least 500ft), there is most of the time a direct path reaching the observers. Therefore, the effects of buildings on propagation are not considered in the following.

Real traffic data

In order to perform realistic environmental impact assessment, the computational tool must be able to handle really-flown trajectory data and assess its noise footprint. Traffic data is always provided in the WGS84 coordinate system, which is consistent with the simulation environment presented in the previous subsection. There exist different ways to get such traffic data. The most used source of traffic data is the Automatic Dependent Surveillance Broadcast (ADS-B) data. However, some rotorcraft are not equipped with the required device. For rotorcraft fitted with a mode S transponder, traffic data can also be retrieved from the communications between that transponder and Secondary Surveillance Radar (SSR). Otherwise, there is also the possibility for customers to provide directly trajectory data recorded by rotorcraft avionics.

In addition, the tool has been upgraded to be able to process multiple trajectories so as to perform more large scale studies on the noise impact of rotorcraft operations. In this case, the helicopter type information is necessary to know which noise source has to be considered for each individual trajectory. For simplicity, in this paper a single rotorcraft type is assigned to all the trajectories evaluated. Future work will address the assignment of the most representative source to every individual trajectory.

Figure 14 shows the noise footprint associated to a 2019 full day of helicopter traffic above Toulouse area (France). The simulations were performed with real track data, but considering only one rotorcraft noise source: H130. We notice two hot

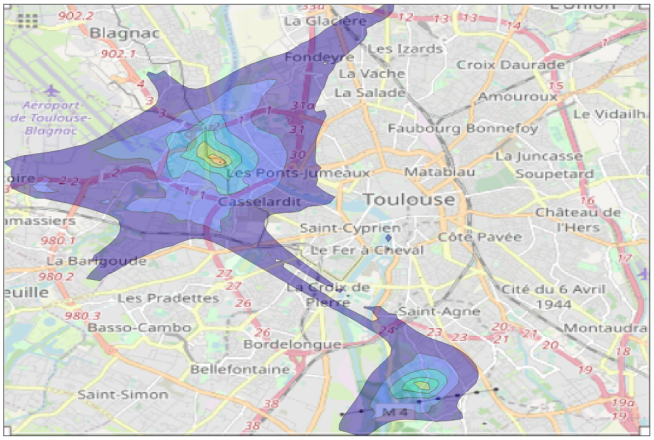

(a) $L_{A,eq}$, 5dB(A) contours

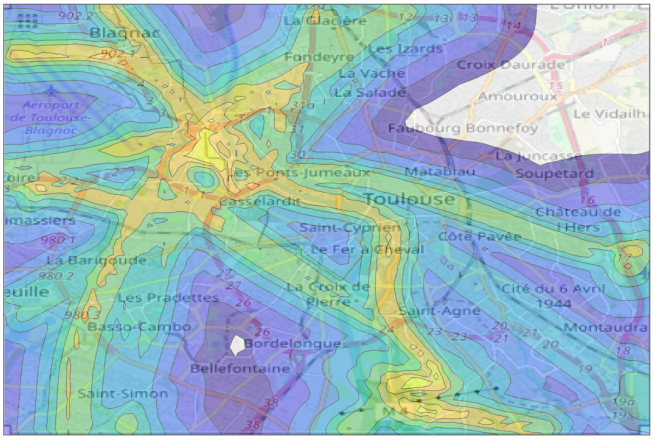

(b) Maximum A-weighted noise level, $L_{A,max}$, 5dB(A) contours

Figure 14. Noise footprint associated to May, 19th 2019 rotorcraft traffic above Toulouse area.

spots from/to which traffic converges: Purpan and Rangueil hospitals, meaning that on that day most of the missions were EMS. Figure 14a shows the general pattern of noise exposure through $L_{A,eq}$ indicator, whereas Figure 14b shows the $L_{A,max}$ contours received during the considered day. The noise levels (not shown here) associated to such rotorcraft traffic suggest the need to further reduce noise exposure by proposing low-noise trajectories.

Demography

In order to minimize rotorcraft traffic noise impact, it is essential to be able to measure the population affected. In that context, the computational chain has been upgraded to link the computed noise footprint to population data. In this paper, we focus on realistic traffic scenarios above France only, for which demographic data is made publicly available by the French National Institute of Statistics and Economic Studies (INSEE). Data is given in a 200m-step grid format, providing the number of inhabitants and population density in each individual (200x200m) cell. In the computational chain, the population density is estimated at each relevant ground position thanks to interpolation of INSEE data. The combination of such data with noise levels allows us to compute a vari-

ety of noise indicators. As an example, Figure 15b shows the number of people affected by a $L_{A,max}$ value above different thresholds.

Such information makes the environmental impact assessment more concrete. Additionally, this information could be used by operators and local players to study the correlation between the complaints and the real noise impact on population. In the scope of designing low-noise trajectories, this is interesting so that we can focus on minimizing the number of people impacted rather than noise areas. The objective function considered in our problem is defined accordingly in the next section.

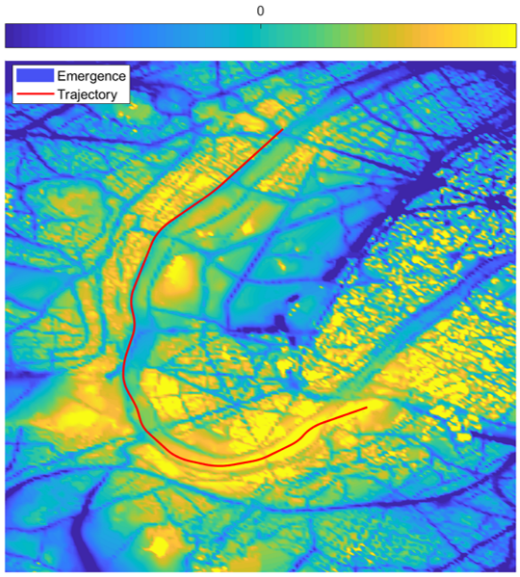

(a) Noise emergence above background noise

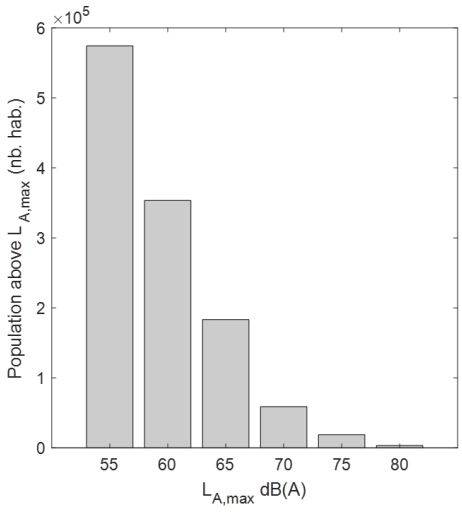

(b) Impacted population over $L_{A,max}$.

Figure 15. A representation of the various noise metrics computed through CAROT.

Background noise

Instantaneous noise metrics, such as $L_{A,max}$ (see Figure 14b) are interesting to show some noise peaks that has non-negligible impact on noise annoyance. However, it is known that the annoyance strongly depends on the surrounding environment where the observer is placed. For the same $L_{A,max}$ value, an observer located in a quiet place (e.g. in a park) could be deeply annoyed, whereas another observer located in a noisy environment (e.g. close to a highway) could even not notice the rotorcraft. Therefore, it is of interest to look at the emergence of given noise events above background noise when trying to minimize rotorcraft noise exposure, keeping in mind that adding more noise to already highly-exposed areas can also be critical. At this stage, background noise information gathering road, rail and aircraft noise is publicly available as L_{den} values for some specific regions only. The data format is similar to the one of demographic data but with a higher resolution (5x5m). Figure 15a shows the emergence above background noise, computed as the difference between $L_{A,max}$ noise level due to rotorcraft overflight and the L_{den} value of ambient noise. Other type of background noise data (e.g. $L_{A,eq}$) could be preferably used if available.

OPTIMIZING ROTORCRAFT TRAJECTORIES

Problem statement

In this paper, we address the low-noise rotorcraft trajectory design as a trajectory optimization problem. An optimization problem consists of three basic elements that are introduced in this section: the decision variables (here presented together with the trajectory modeling), the objective (cost) function to be minimized, and the constraints.

Trajectory modeling In this paper, a trajectory is modeled as a set of successive waypoints $\mathscr{W}$. Each individual waypoint $w \in \mathscr{W}$ is defined by the rotorcraft 3D position x_w, y_w and z_w and its ground speed norm v_w, leading to a quadruplet $(x_w, y_w, z_w, v_w) \in \mathbb{R}^4$. A realistic smooth and flyable trajectory is determined afterwards from the interpolation of these waypoints. In particular, trajectories are built as a succession of straight segments and circular arcs between the waypoints. As depicted in Figure 16, the trajectory does not necessarily pass over each waypoint. The number of waypoints $N_{\mathscr{W}}$ is a data of the problem, whose value depends on the instance considered. The decision variables are the degrees of freedom used to design a trajectory with a minimal noise impact. In this paper, the decision variables are the 4-dimensional coordinates defining the waypoints.

The number of decision variables is strictly less than $4N_{\mathscr{W}}$, since some of the waypoints ground speeds or 3D coordinates are user-fixed. As an example, the initial (x_0, y_0, z_0, v_0) and final (x_f, y_f, z_f, v_f) waypoints are always fixed prior to optimization. The waypoints are originally defined according to obstacles and their number has to be chosen carefully. On the one hand, there must be enough waypoints to model and optimize complex trajectories. On the other hand, the more the waypoints, the more the decision variables and more complex

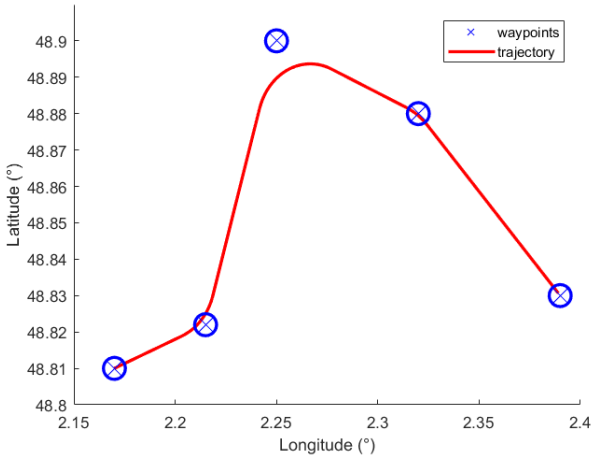

Figure 16. A smooth trajectory (red line) is built by special interpolation of waypoints (blue dots).

the optimization. Too many waypoints can have a detrimental effect on the computing time for optimization, while showing negligible improvement of the solution.

Cost function The objective (cost) function, which has to be minimized, characterizes the acoustic performance of the proposed low-noise rotorcraft trajectory. Therefore, it has to be derived from a typically used noise metric. In this paper, as we focus on optimizing single trajectories, single-event noise metrics are considered. Such metrics can be either instantaneous (e.g. $L_{A,max}$) or time-integrated (e.g. Sound Exposure Level). The choice of the metric can lead the optimizer to propose very different solutions, as detailed in (Ref. 3). Typically, minimizing instantaneous noise metrics can be achieved by reducing the rotorcraft speed, whereas minimizing time-integrated noise metrics would lead the optimizer to increase the rotorcraft speed in order to reduce its overflying duration. In addition, as detailed in the previous section, many other noise metrics can be computed through the computational chain, in particular including demographic data.

In this paper, the objective function is based on the Sound Exposure Level (SEL), so that the time exposure is taken into account. For optimization purpose, all the computed noise levels are converted into one single value that has to be minimized. This value can simply be obtained by averaging SEL levels on the whole grid. In order to avoid getting very fast trajectories characterized by noise levels which are locally high, the cost function will be a weighted average of SEL noise levels. This could be achieved by computing the power average (i.e. the average over quadratic pressure). In this case, the cost function would strongly depend on the highest noise levels, almost neglecting the lowest levels of the grid. The optimization would then be driven by ground locations that stay very close to the rotorcraft, and would propose solutions that minimize the noise mainly under the flight track when the rotorcraft is close to the ground. In order to avoid this effect, a more appropriate weighting applied to SEL levels is introduced in the following. In addition, as the tool used for noise computation (CAROT) has been coupled with demographic data, the number of people receiving the computed SEL noise levels will be minimized rather than minimizing these noise levels directly.

The cost function f considered in this paper is defined as follows. Let N_m be the total number of relevant ground locations where the noise level has been computed. For all $k \in \{1,2,\ldots,N_m\}$, let $\mathrm{SEL}(k)$ be the SEL noise level computed at ground location k and p_k be the number of people associated to this location. The total population considered for a given trajectory assessment is denoted p_{tot} and defined as:

$$p_{tot} = \sum_{\substack{k\in[1,N_m]:\\ \mathrm{SEL}(k)\geq\mathscr{L}_1}} p_k \tag{1}$$

where $\mathscr{L}_1 = 70\mathrm{dB(A)}$ is the first element of the considered set of SEL noise levels defined as $\mathscr{L} = \{70,75,80,85,90,95,100\}$ dB(A).

For all $i \in \{1,2,\ldots,|\mathscr{L}|\}$, let $\mathscr{M}_i$ be the subset of ground locations, whose SEL noise level is in $[\mathscr{L}_i,\mathscr{L}_{i+1}[$. Its expression is given below:

$$\mathscr{M}_i = \{k \in [1,N_m], \mathscr{L}_i \leq \mathrm{SEL}(k) < \mathscr{L}_{i+1}\}. \tag{2}$$

P_i denotes the number of people receiving a SEL level between $\mathscr{L}_i$ and $\mathscr{L}_{i+1}$, and is defined as:

$$P_i = \frac{1}{|\mathscr{M}_i|} \sum_{k\in\mathscr{M}_i} \frac{p_k}{p_{tot}} \tag{3}$$

Finally, the objective function to be minimized is the weighted sum of the population impacted by different SEL noise levels and defined as:

$$f = \sum_{i=1}^{|\mathscr{L}|} \alpha_i * P_i \tag{4}$$

The weighting factors $\alpha_i \geq 1, i \in \{1,2,\ldots,|\mathscr{L}|\}$ are user-defined parameters, which are fixed at the beginning of the optimization. In this way, the user can choose to give more or less value to the different SEL noise levels.

Constraints The constraints that apply to the considered problem are mainly based on operational requirements. The trajectory must respect Air Traffic Management (ATM) regulations, such as obstacle avoidance with respect to a given margin. Lower and upper bounds are imposed to all the position variables (x, y and z) so that the variable space remains out of obstacles. Contrary to the work presented in (Ref. 3), this paper assumes that rotorcraft trajectories are flown under Visual Flight Rules (VFR). It means that rotorcraft are operated in Visual Meteorological Conditions (VMC). In this framework, pilots are able to fly using visual reference only instead of relying on instruments like in Instrument Flight Rules (IFR) operations. Therefore operational constraints relative to VFR are less restrictive. The constraints are thus mostly imposed by rotorcraft performance limitations (e.g. maximum rate of turn, maximum TAS). A minimum TAS of 50kt is set to avoid Vortex Ring State (VRS) domain. Several constraints are also

defined to ensure passenger comfort and limit pilot workload. The numerical values considered in this paper are the following: the rate of descent shall not exceed 1200ft.min^{-1}, the descent slope is limited -12° and acceleration/deceleration must not exceed 3kt.s^{-1}.

Algorithmic scheme

The values of the number of people seeing the different SEL noise levels ($P_i, i \in \{1, 2, \ldots, |\mathscr{L}|\}$) are computed through the computational chain presented previously. From the optimization point of view, the computational chain behaves like a black-box that takes as an entry a candidate solution (i.e. a rotorcraft trajectory) and outputs the associated objective function value and the evaluation of the constraints. Due to the complex treatments done by the computational software, we do not have access to any analytical expression of the objective function f in terms of the decision variables. The analytical expression of the derivatives of f is not available either, and cannot be approximated through finite differences due to the computational cost that would be induced. Therefore, the optimization problem described above belongs to the class of Black-Box Optimization (BBO) problems.

Solution algorithms for solving BBO problems do not rely on gradient information to compute descent directions. Among them, heuristic methods, especially population-based algorithms, have been widely used to solve BBO problems (Refs. 3, 4). Such methods are generally computationally expensive since the black-box is called at each iteration for the evaluation of each individual of the population. Despite the improvements in the efficiency of the noise footprint computational chain detailed in previous sections, the evaluation of a single candidate solution is still computationally expensive (approx. 10s on average as shown in Table 2). Therefore, population-based methods are not used in this paper. We focus on methods that can provide at least a guarantee of local optimality, such as direct search methods that are based on the exploration of the search space according to predefined directions of search. In this paper, we resort to a state-of-the-art method, that is known to efficiently solve BBO problems with a guarantee of local optimality: the Mesh-Adaptive Direct Search (MADS) (Ref. 19). It is applied through the NOMAD (Ref. 20) implementation software.

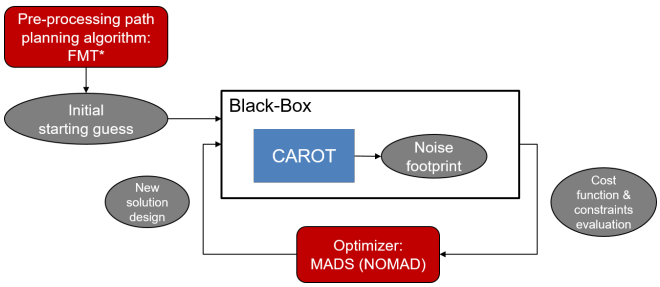

Figure 17. Proposed algorithmic scheme.

The general functioning of the optimization algorithm is described in Figure 17. At the beginning, the user must provide an initial solution (i.e. a rotorcraft trajectory). Then, at each iteration, a new candidate solution is proposed by the MADS algorithm. This new design is evaluated through the black-box, which returns the values of the associated cost function and of the constraints. These values are then used by the MADS algorithm to propose another new solution. This process is repeated until reaching a stopping criterion, that has been pre-defined by the user. In this paper, the algorithm stops after ten consecutive failed iterations of the MADS.

The MADS algorithm has been enhanced to efficiently solve the problem of minimal noise trajectory design. In particular, as MADS is a local optimization method, the optimal computed solution closely depends on the choice of the initial candidate solution. It is thus necessary to provide NOMAD with the best possible starting guess, which has to be feasible with respect to the problem constraints. This initial trajectory is composed of a 3D path, which results from an auxiliary path planning problem. A speed profile is assigned to the obtained 3D path afterwards to stick to the constraints. The generation of such initial candidate must stay limited in terms of computational time, since it is only the starting point of the whole optimization process. Therefore, the noise footprint computational chain will not be used at this stage. The criterion guiding the search of the optimal 3D path is mainly based on population overflown. In order to avoid getting unrealistically long paths, the distance travelled is added to the criterion. The objective function, which is minimized, is then a convex weighted sum of distance travelled and population exposure. The 3D optimal path is computed through an asymptotically optimal path planning algorithm: Fast Marching Tree (FMT*) (Ref. 21). Figure 18 shows the optimal 3D path obtained for two different weighting. The blue path focuses on reducing the population overflown while the black one favors the reduction of the path length.

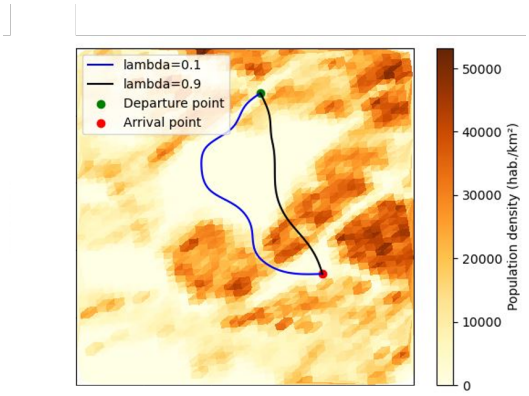

Figure 18. 2D upper view of the optimal path computed through FMT* algorithm, over population density.

Once a first initial trajectory solution is computed through the above mentioned path planning algorithm (FMT*), the search space is reduced to a *corridor* around this initial guess. This corridor is defined in such a way that it remains out of obstacles, as illustrated in Figure 19a. The optimization algorithm

then browses such corridor to find the trajectory minimizing the noise exposure.

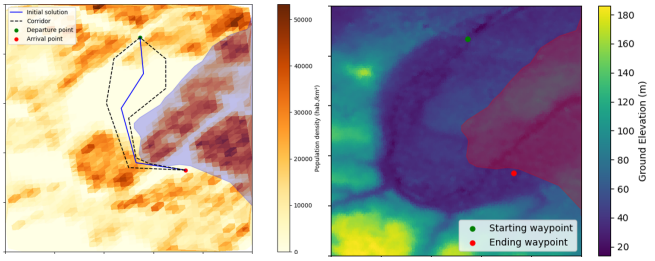

(a) 2D population density upper view. The higher the population density, the browner.

(b) 2D ground elevation upper view. The higher the ground, the yellower.

Figure 19. Illustration of the environmental characteristics of the first test case.

RESULTS

In this section, we address two realistic test cases that have been built on real-world rotorcraft traffic examples, retrieved from radar data. These rotorcraft trajectories have been optimized through the algorithmic scheme and noise footprint computational chain presented in the previous sections. For all the test cases, we compare the optimal trajectory proposed by our method to the really-flown trajectory (referred to as reference trajectory). All the numerical tests have been performed on a Linux platform with 48 CPUs (3.00 GHz) and 130 GB RAM.

The first instance corresponds to a cruise and approach flight to a particular heliport located in a highly-densely populated area. Such area is particular due to the presence of no-fly zones considered as obstacles. They are represented in blue over population density (see Figure 19a) and in red over terrain elevation data (see Figure 19b). The search space, defined as a corridor around the first initial guess, is illustrated in dashed black on Figure 19a.

First, we assessed the potential gains that might be obtained by optimizing the vertical profile only, i.e. the lateral path has been kept fixed and identical to the lateral path of the reference trajectory. Only the rotorcraft altitude z and speed v are considered as decision variables in the optimization process. The predicted noise reduction is depicted in Figure 20a, which shows the difference in SEL noise levels (3dB(A) noise contours) between the proposed optimal and the reference trajectories over the population density, displayed in shade of gray. We observe that significant gains up to 6dB(A) locally can be achieved by optimizing the vertical profile only. This result is consistent with previous studies (Refs. 3, 4) made on hypothetical approach flights. Figure 20a also shows that there exists some local areas, where the predicted noise of the proposed optimal trajectory is higher (up to 3dB(A) locally) than that of the reference one. Such acoustic losses are the result of a compromise to achieve global noise reduction on the whole area considered. In particular, we remark that the losses occur in areas where the population density is lower than that of areas where the gains are achieved.

In addition to the optimization of vertical profiles, the solution approach presented in the preceding sections is able to provide trajectories that are optimized in 4D. The noise reduction predicted with the proposed 4D optimal trajectory with respect to the reference one is depicted in Figure 20b. We observe huge acoustic gains and losses in the area under study due to the modification of the lateral path. Even though the losses appear to be huge, they occur in areas where the population density is relatively low. Besides, the predicted gains occurs in highly-densely populated areas, achieving a global reduction of impacted population.

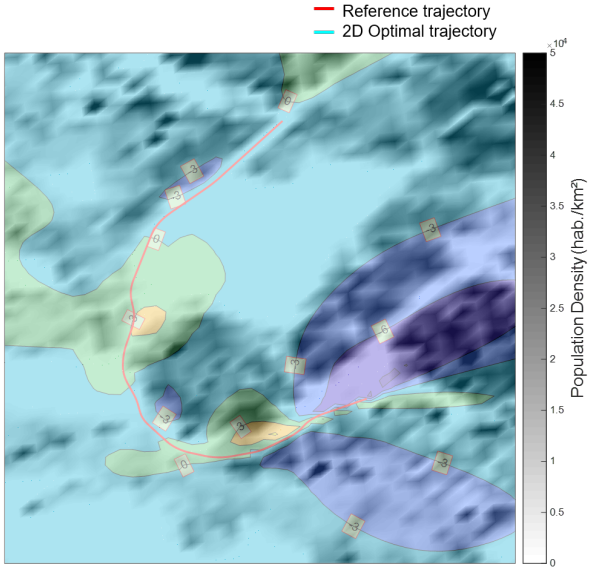

(a) ΔSEL(2D Optimal trajectory) - SEL(Reference trajectory).

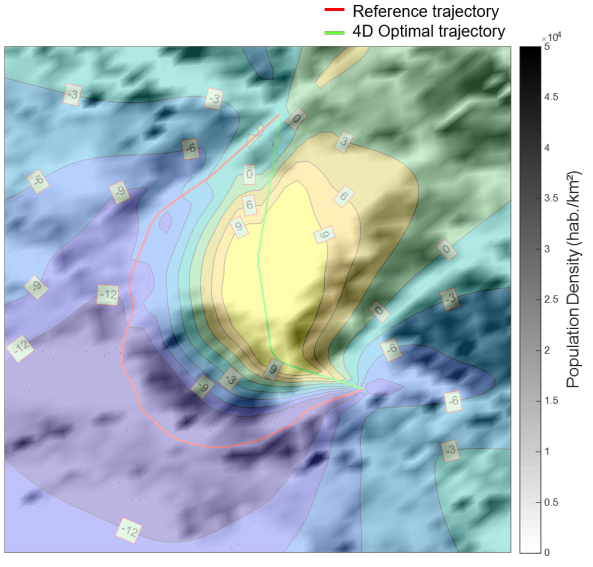

(b) ΔSEL(2D Optimal trajectory) - SEL(Reference trajectory).

Figure 20. Predicted noise difference between different optimal (2D, 4D) trajectories and the reference one.

Figure 21 details the overall reduction of the population noise

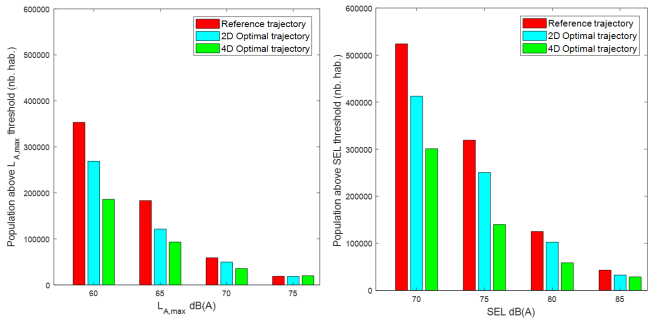

(a) Population affected by $L_{A,max}$ values above given thresholds.

(b) Population affected by SEL values above given thresholds.

Figure 21. Predicted population noise exposure for different metrics ($L_{A,max}$, SEL).

Optimization framework	$L_{A,max}$ dB(A)			
	60	65	70	75
2D Optimal	24%	34%	15%	2%
4D Optimal	47%	49%	39%	-5%

Table 3. Overall population noise exposure reduction ($L_{A,max}$) predicted with the proposed optimal trajectories.

Optimization framework	SEL dB(A)			
	70	75	80	85
2D Optimal	21%	21%	18%	24%
4D Optimal	43%	56%	53%	33%

Table 4. Overall population noise exposure reduction (SEL) predicted with the proposed optimal trajectories.

exposure for the two different optimal trajectories with respect to the reference one. It depicts the number of people impacted for different threshold values of $L_{A,max}$ and SEL. Figure 21, Tables 3 and 4 show that higher noise exposure reductions can be achieved by modifying both the lateral path and the vertical profile of the trajectory considered. As an example, we predict a 53% (respectively 18%) reduction of the number of people impacted by a SEL value higher than 80dB(A) for the 4D optimal trajectory (resp. 2D optimal trajectory).

The evolution of the rotorcraft noise dependent flight parameters (altitude, TAS and flight path angle) is given in Figure 22 in function of the distance to the expected landing point. We observe in particular that the 2D optimal trajectory proposes a steeper approach (up to -10°) in two steps to avoid the typical flight conditions where Blade-Vortex Interaction (BVI) occurs and to benefit from the geometrical effect.

The second instance differs from the first one on the underlying simulation environment. This test case corresponds to the optimization of a rotorcraft cruise and approach flight to a particular heliport located on the sea shore. Indeed, the population distribution is very different from the first test case as it combines both very high density areas (on the coast) and uninhabited areas (above the sea) as represented in Figure 23a. Ground elevation is also illustrated for this instance in Figure 23b.

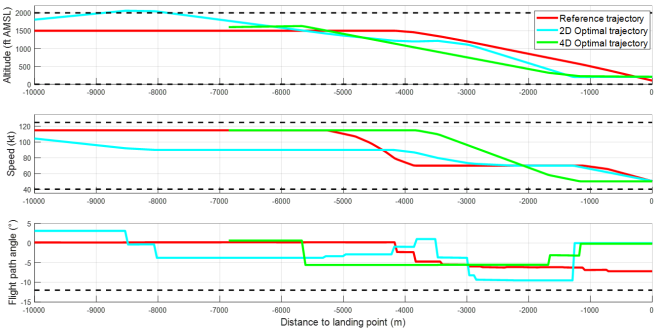

Figure 22. Comparison of the noise dependent flight parameters between the optimal and reference trajectories.

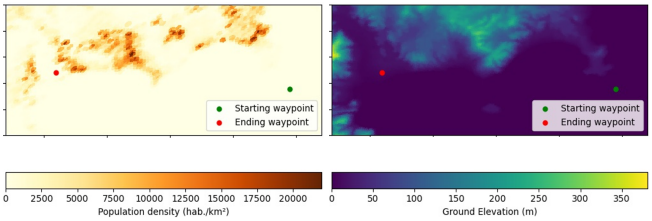

(a) 2D population density upper view. The higher the population density, the browner.

(b) 2D ground elevation upper view. The higher the ground, the yellower.

Figure 23. Illustration of the environmental characteristics of the second test case.

As the environment is less constrained than for the first instance, we present the result for the 4D optimal trajectory only. Figure 24 shows the predicted noise reduction (3dB(A) SEL contours) obtained with the optimal trajectory with respect to the reference one. We can see that some huge acoustic losses (up to 9dB(A)) occur mainly above the sea, having a very limited impact on population. The overall noise reduction is achieved by the gains obtained (up to 12dB(A)) close to the landing site, where the population density is much higher. The temporal evolution of the flight parameters is also given in Figure 25. The proposed approach is less steep than the one proposed in the first case. Indeed, we remark that the 2D lateral path is modified so that the rotorcraft is pushed away from highly-densely populated areas (see Figure 24. It is thus not as necessary to perform a steep approach since the rotorcraft overflies inhabited areas. Additionally, we can see a quite long ($\sim$ 2000m) final leg at low altitude, which is not detrimental in this case since the rotorcraft approaches the landing point from the see.

Figure 26 shows that significant reduction can be achieved on population noise exposure for both $L_{A,max}$ and SEL noise metrics. In particular, we remark that the number of people impacted for the different noise levels is much lower than for the first case as this example considers an area with a lower population density.

These two instances retrieved from real-world operations show that significant noise exposure reduction can be achieved by flying differently. The proposed approach shows that the highest acoustic gains can be obtained by modifying both the lateral path and the vertical profile of the considered

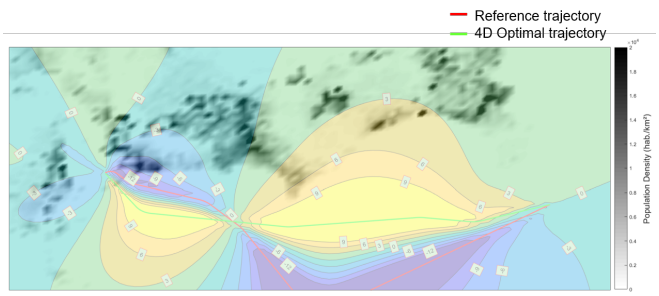

Figure 24. ΔSEL(Optimal trajectory) - SEL(Reference trajectory). Predicted noise difference (SEL) between the optimal trajectory and the reference one.

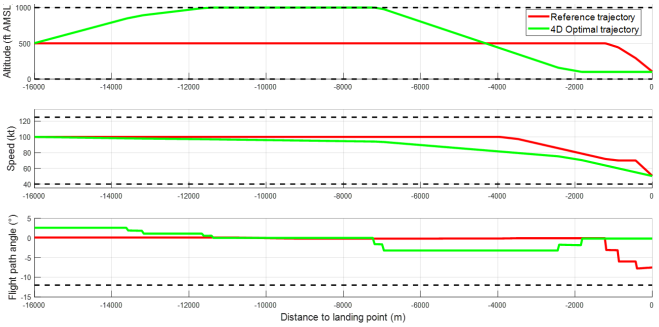

Figure 25. Comparison of the noise dependent flight parameters between the optimal and reference trajectories.

rotorcraft trajectory. However, in highly constrained environment (e.g. in urban areas), there might be no possibility to modify the lateral path for safety reasons. In this case, we showed through the first instance that significant gains can still be achieved by optimizing the vertical profile only. The proposed approach shows significant noise reduction for both instantaneous ($L_{A,max}$) and time-integrated (SEL) noise metrics. This potential reduction in noise exposure by modifying the rotorcraft trajectory remains highly dependent on the area considered and the local constraints.

CONCLUSION

An accurate noise footprint computational chain (CAROT) is presented, that is able to perform efficient and realistic environmental impact assessment. This new capability can be used to support operators to be able to assess the noise footprint of their own operations. It might also help authorities to define new operational procedures to reduce rotorcraft community noise impact. This software has been validated through flight tests experiments for the H130 helicopter only. Further work will focus on extending the model to other types of rotorcraft. In particular, this relies on the improvement of the existing noise databases for different rotorcraft types, that can be achieved by numerical simulations or by performing additional flight tests, like for the H130 used in this paper.

A generic methodology is introduced to compute optimal rotorcraft trajectories minimizing their noise footprint. The methodology is applied on a specific type of rotorcraft (H130) but can be used for any type of rotorcraft and even future UAVs, provided that noise sources are available. Such low-noise trajectory design is a possibility for operators to further reduce their operational noise, besides flying with quieter rotorcraft. Perspectives include the generation of multiple alternative paths in case of huge traffic in order to bring more equity to the population exposed to high noise levels.

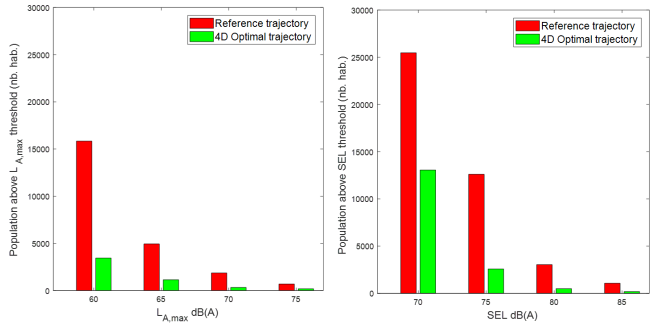

(a) Population affected by $L_{A,max}$ values above given thresholds.

(b) Population affected by SEL values above given thresholds.

Figure 26. Predicted population noise exposure for different metrics ($L_{A,max}$, SEL).

Author contact:
Pierre Dieumegard, pierre.p.dieumegard@airbus.com
Frédéric Guntzer, frederic.guntzer@airbus.com
Julien Caillet, julien.caillet@airbus.com
Sonia Cafieri, sonia.cafieri@enac.fr

ACKNOWLEDGMENTS

The authors wish to acknowledge the Clean Sky 2 Joint Undertaking (CSJU) for the financial support of this research performed in the frame of the Fast RotorCraft RACER project.

The authors also wish to thank Clément Florentin for his personal contribution on the study of the influence of the wind on noise propagation.

REFERENCES

1. Rauch, P., Gervais, M., Cranga, P., Baud, A., Hirsch, J.-F., Walter, A., and Beaumier, P., "Blue Edge™: The Design, Development and Testing of a New Blade Concept," American Helicopter Society 67th Annual Forum, 2011.

2. Guntzer, F., Gareton, V., Pinacho, J.-P., and Caillet, J., "Low Noise Design and Acoustic Testing of the Airbus Helicopter H160-B," 45th European Rotorcraft Forum, September 2019.

3. Guntzer, F., Gareton, V., Gervais, M., and Rollet, P., "Development and testing of optimized Instrument Flight Rules (IFR) noise abatement procedures on EC155," American Helicopter Society 70th Annual Forum, Montreal, Quebec, Canada, May 2014.

4. Padula, S. L., Burley, C. L., Boyd Jr., D. D., and Marcolini, M. A., "Design of Quiet Rotorcraft Approach Trajectories," NASA TM 215771, NASA, 2009.

5. Morris, R., Johnson, M., Venable, K. B., and Lindsey, J., "Designing Noise-Minimal Rotorcraft Approach Trajectories," *ACM Transactions on Intelligent Systems and Technology*, Vol. 7, (4), 2016, pp. 1–25. DOI: 10.1145/2838738

6. Gopalan, G., Xue, M., Atkins, E. M., and Schmitz, F. H., "Longitudinal-Plane Simultaneous Non-Interfering Approach Trajectory Design for Noise Minimization," American Helicopter Society 59th Annual Forum, Phoenix, Arizona, May 2003.

7. Greenwood, E., Schmitz, F. H., and Sickenberger, R. D., "A Semiempirical Noise Modeling Method for Helicopter Maneuvering Flight Operations," *Journal of the American Helicopter Society*, Vol. 60, (2), 2015, pp. 1–13.

8. Greenwood, E., "Dynamic Replanning of Low Noise Rotorcraft Operations," American Helicopter Society 75th Annual Forum, Philadelphia, Pennsylvania, May 2019.

9. Guntzer, F., Spiegel, P., and Lummer, M., "Genetic Optimization of EC-135 Noise Abatement Flight Procedures using an Aeroacoustic Database," 35th European Rotorcraft Forum, Hamburg, Germany, September 2009.

10. Greenwood, E., "Helicopter Flight Procedures for Community Noise Reduction," American Helicopter Society 73rd Annual Forum, May 2017.

11. Olsman, W., and Lummer, M., "Influence of wind on the noise footprint of a helicopter landing," 38th European Rotorcraft Forum, Amsterdam, Netherlands, September 2012.

12. Spiegel, P., Buchholz, H., and Pott-Pollenske, M., "Highly Instrumented BO105 and EC135-FHS Aeroacoustic Flight Tests including Maneuver Flights," American Helicopter Society 61st Annual Forum, June 2005.

13. Greenwood, E., Schmitz, F. H., Gopalan, G., and Sim, B. W.-C., "Helicopter External Radiation in Turning Flight: Theory and Experiment," American Helicopter Society 63rd Annual Forum, May 2007.

14. Chen, H.-N., Brentner, K. S., Shirey, J. S., Ananthan, S., and Leishman, J. G., "A study of the Aerodynamics and Acoustics of Super-BVI," American Helicopter Society 62nd Annual Forum, May 2006.

15. Benoit, B., Dequin, A.-M., Kampa, K., Gruenhagen, W., Basset, P.-M., and Gimonet, B., "HOST: a general helicopter simulation tool for Germany and France," American Helicopter Society 56th Annual Forum, May 2000.

16. Beaumier, P., and Delrieux, Y., "Description and validation of the ONERA computational method for the prediction of blade-vortex interaction noise," *Aerospace Science and Technology*, Vol. 9, (1), 2005, pp. 31–43. DOI: 10.1016/j.ast.2004.07.008

17. Marze, H.-J., Gervais, M., Martin, P., and Dupont, P., "Acoustic flight test of the EC130 B4 in the scope of the Friendcopter project," 33rd European Rotorcraft Forum, September 2007.

18. Bocher, E., Guillaume, G., Picaut, J., Petit, G., and Fortin, N., "NoiseModelling: An Open Source GIS Based Tool to Produce Environmental Noise Maps," *ISPRS International Journal of Geo-Information*, Vol. 8, (3), 2019. DOI: 10.3390/ijgi8030130

19. Audet, C., and Dennis, J. E., "Mesh Adaptive Direct Search Algorithms for Constrained Optimization," *SIAM Journal on Optimization*, Vol. 17, (1), 2006, pp. 188–217. DOI: 10.1137/040603371

20. Le Digabel, S., "Algorithm 909: NOMAD: Nonlinear Optimization with the MADS Algorithm," *ACM Transactions on Mathematical Software*, Vol. 37, (4), 2011, pp. 1–15. DOI: 10.1145/1916461.1916468

21. Janson, L., Schmerling, E., Clark, A., and Pavone, M., "Fast marching tree: A fast marching sampling-based method for optimal motion planning in many dimensions," *The International Journal of Robotics Research*, Vol. 34, (7), 2015, pp. 883–921. DOI: 10.1177/0278364915577958